PCCP

Accepted Manuscript

ROYAL SOCIETY OF CHEMISTRY

www.rsc.org/pccp

PCCP

RSCPublishing

ARTICLE

Molecular Dynamics Simulations Reveal the Assembly Mechanism of Polysaccharides in Marine Aerosols

Cite this: DOI: 10.1039/x0xx00000x

Received 00th January 2014,
Accepted 00th January 2014

DOI: 10.1039/x0xx00000x

www.rsc.org/

Lu Sun [a], Xin Li [a], Thomas Hede[b], Yaoquan Tu [a], Caroline Leck[b], Hans Ågren[a] *

ABSTRACT. The high Arctic marine environment has recently detected polymer gels in atmospheric aerosol particles and cloud water originating from the surface microlayer of the open leads within pack ice area. These polysaccharides molecules are water insoluble but water solvated, highly surface-active and highly hydrated (99% water). In order to add to the understanding and to complement missing laboratory characterization of marine polymer gels we have in this work performed an atomistic study on the assembly process and interfacial properties of polysaccharides. Our study reveals a number of salient features of the microscopic process behind polysaccharide assembly into nanogels. With three- and four-repeating units the polysaccharides assemble into a cluster in 50ns. The aggregates grow quicker by absorbing one or two polymers each time, depending on unit length and type of inter-bridging cation. Although both the hydrophobic and hydrophilic domains are contracted, the latter one dominates distinctly on the contraction of solvent accessible surface areas. The establishing of inter-chain hydrogen-bonds is the key to the assembly while ionic bridges can further promote the aggregation. During assembly of the more bent four-unit polymers, intra-chain hydrogen bonds are significantly diminished by Ca^{2+}. Meanwhile, the percentage of Ca^{2+} acting as ionic bridges is more eminent, highlighting the significance of Ca^{2+} ions for longer-chain polysaccharides. The aggregates are able to enhance surface tension more in the presence of Ca^{2+} than in the presence of Na^{+} owing to the more compact structure. These conclusions all demonstrate that studies of the present kind provide insight into the self-assembly process and interfacial properties of marine gels. We hope this understanding will keep up the interest of the complex but fascinating relationship between marine microbiology, atmospheric aerosols, clouds and climate.

1.Introduction

Clouds remain an uncertainty in the parametrization of General Circulation Models (GCM´s) which are commonly in use to give projections of future climate change.[1] The concentration of cloud water drops is largely determined by the concentration of particle nuclei on which cloud drops can form (cloud condensation nuclei, or CCN).[2] This also requires that the meteorological conditions, wind, humidity and temperature are favorable. Surface-active properties of the CCN are able to lower the surface tension and promote the condensational growth of cloud droplets once formed, while hydrophilic elements enhance the surface tension and increase the number concentration of activated droplets.[3] Airborne primary particles in sizes of a CCN originate over the remote ocean from a variety of sources located at the surface microlayer (< 100 μm thick at the air-sea interface) or from the bulk water below.[4]
The surface microlayer of oceans is enriched with dissolved organic carbons (DOCs), which are primarily produced by phytoplankton or as secretion of bacteria.[5] These DOCs are either truly dissolved (<1 nm) or colloidal (1~1000nm).[6] By a transmission electron microscopy (TEM) study, Leppard et al.[6] observed that fractal aggregates (1~60nm) dominate over a wide range of marine colloidal particles. Santshi et al.[7] utilized

combined TEM and atomic force microscopy (AFM) to scan particles down to as small as 1 nm and found fibril polysaccharides with different size to be abundant near the surface of seawater. The organic material is typically solved in a thin viscous film at the atmosphere/ocean interface and is capable of undergoing self-assembly and aggregation into marine nano- and micro-gels.[8] The size range of marine gels is between a few nano-meters in diameter up to gels of aggregates of several hundreds of μm.[9] Moreover, gels in micro-meter sizes are probable to be injected into the air with film drops and jet drops during bubble bursting at the air-sea interface.[10] The detection of organic substances specifically of polymer like particles in the atmosphere was first discovered by Bigg and Leck. These authors recognized that these particles could bear the physicochemical characteristics of marine gels. This followed from their studies of a possible link between cloud formation and polymer gels in the surface microlayer in the high Arctic sea ice.[12] It has been additionally shown by Bigg that organic carbon is predominant concerning mass concentration, even higher than sea-salt, on the west coast of Ireland during phytoplankton blooming.[13] Recent unique results confirm for the first time that polymer gels in atmospheric aerosols particles and in cloud water originate from the ocean surface microlayer. [14] High Arctic new particle formation in distinct size ranges coincide with particles in the 20-50 nm diamter size range, but cannot be expained by secondary particle formation.[15] The release of so called nano-granules (nanogel polymers) from evaporating fog/cloud droplets may be crucial to the formation of nano-sized particles in the Arctic summer.[16]

Imbedded in solvents water, marine polymsaccharides assemble into gels through weak physical bonds or tangles.[9] The stability of the gels are strikingly dependent on whether the chains are polyelectrolytes, the concentration of the polymers, their charge density, and on the ratio of hydrophobic/hydrophilic domains.[9] If the polymers possess chains as polyelectrolytes, they are probable to form complexes with their multivalent counterions and come out as cross-linked structures.[17] The cross–linked conformation will also be formed when hydrophobic domains interact with each other through tangles. Owing to the presence of uronic acid and sulfonic acid, sampled polymers show a net negative charge where the presence of Ca^{2+} is influential.[18] Experiments have shown that gels are destabilized after chelating Ca^{2+} by ethylenediamminetetraacetate (EDTA).[14b] Furthermore, previous simulations have indicated the formation of ionic bridges during the assembly process.[17] Nevertheless, the influence of ionic bridges is not so prominent on the dynamics for the short-chain assemblies.

To build knowledge beyond previous studies and gain insight into the assembly process of polysaccharides and the conformations of nanogels[9], we perform in this work molecular dynamics simulations on sugar polymers with focus on the interfacial properties of gels promoting or suppressing cloud droplet formation in marine environments.

2 Computational details

Molecular dynamics simulations were carried out employing the GROMACS package for a series of systems to study the ion effect on the aggregation and interfacial properties.[19] Since the laboratory measurements have determined the presence of glucuronofucan, the polysaccharides are built as Scheme 1, where 25% of the monosaccharides are charged.[20] Moreover, on one hand, Verdugo et al propose that the abundant dissolved organic matter in seawater possess a median molecular weight of 2~3 kDa with their length being at the scale of several nanometers.[21] One the other hand, Ewalds proposed that the assembly dynamics could speed up more than one order of magnitude on the increase of length.[22] We hereby construct polysaccharides comprising of 3 and 4 repetition units, with molecular weight of 1.9 kDa and 2.5 kDa, respectively. The difference in length enables a comparison of the assembly dynamics.

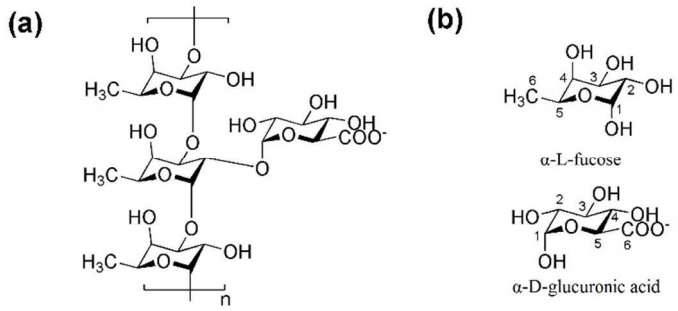

Scheme 1. (a) The structure of a unit of the polysaccharide, the overall length of the chain is determined by the number of repetition, n. (b) Each unit consist of three α-L-fucose and one α-D-glucuronic acid.

The initial configuration of a system is constructed by inserting 10 polymer chains randomly into a 10×10×10 box, followed by solvating them with water molecules. Ions were subsequently inserted with the number listed in Table 1. The concentration of Ca^{2+} and Na^{+} was subsequently controlled at 0.086 mol L^{-1} and 0.340 mol L^{-1} by enlarging the box and adding more solvent molecules. The GLYCAM force field, which is reported to reproduce the rotamer populations and to be suitable for carbohydrates, was employed for polysaccharides together with the AMBER force field for ions and the TIP3P model for water.[23] Simulations were carried out after energy minimization and a periodic boundary condition (PBC) was applied. The NPT ensemble was used in the simulation with temperature maintained at 298 K by the velocity rescaling thermostat and pressure coupled to 1 bar by the Berendsen barostat.[24] Bonds containing hydrogen atoms were constrained by the LINCS algorithm.[25] The long-range Coulombic interactions were remedied by the PME method with the cut-off radius set at 1.2 nm.[26] Each simulation was carried out for 100 ns with a time-step of 2 fs. After the assembly process, the z-axis of each box was elongated by 3nm both upside and downside to create surface area. The simulation continues from the assembled configuration for another 100 ns without barostat.

Table 1. Composition of the systems studied.

System	PS	COO^-	Ca^{2+}	Na^+	Cl^-	L_{box}
$PS_{n3} + Ca^{2+}$	10	30	60	0	90	10.51
$PS_{n3} + Na^+$	10	30	0	240	210	10.52
$PS_{n4} + Ca^{2+}$	10	40	80	0	120	11.56
$PS_{n4} + Na^+$	10	40	0	320	280	11.57

3 Results and discussion

3.1 Assembly dynamics of polysaccharides

Imbedded in the solvent, the polysaccharide molecules attract each other and the self-assembly process initiates. The largest aggregate keeps absorbing other polysaccharides and becomes the maximum cluster within the first 50 ns, as shown in Fig 1(a) and (b). It takes approximately 40 ns for the four-unit polysaccharides(PS_{n4}) to aggregate into the maximum cluster, which comprises of ten polymers. It is noting that assembly is promoted in the presence of Ca^{2+} and the largest cluster of polysaccharides reaches the size of nine polymers within the first 20 ns, indicating that the aggregation of long chain polymers is accelerated by Ca^{2+}. This acceleration is much more dominant compared with that for three-unit polysaccharides(PS_{n3}). Moreover, that the increase in length of the polysaccharides favors aggregation is observed in the presence of Ca^{2+}. Nevertheless, it is interesting that the aggregation rate of the elongated chain is little affected with Na^+ as counterions. It is worthwhile to note that for PS_{n3} in the presence of Na^+, the size of the largest cluster increases gradually instead of a sudden surge. This process is quicker than forming smaller clusters and merging them all of a sudden. In this respect, in the presence of Na^+, it takes less time for PS_{n3} to aggregate into the maximum cluster than PS_{n4}, as shown in Fig 1(b).

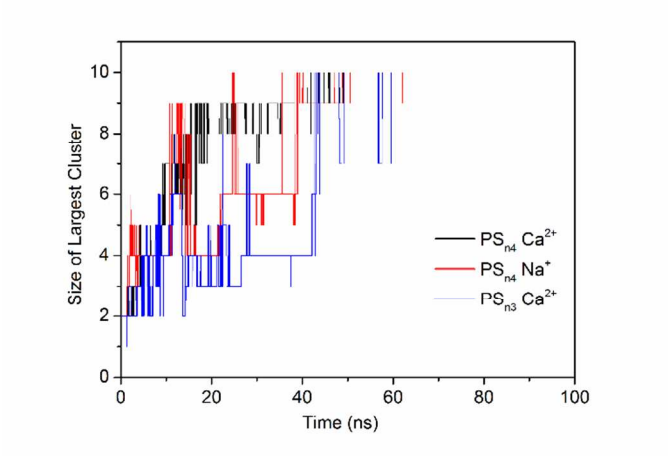

(a)

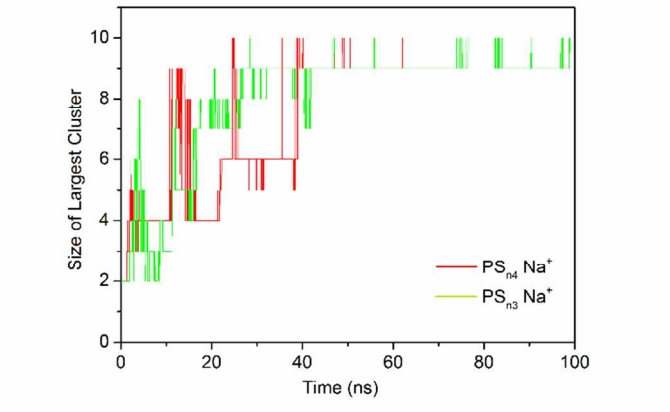

(b)

Figure 1. Number of the polysaccharides in the largest cluster. Different length and different cations influence the assembly process.

With the polymers approaching each other and undergoing self-assembly, the solvent accessible surface area (SASA) diminishes, as seen in Fig 2(a). For each system, an apparent decrease of the SASA is observed during the first 50 ns, which is the time corresponding to the cluster growth. The overall SASA of each assembling system is observed a contraction of approximately 23%. The average decreasing rates of SASA for PS_{n4} and PS_{n3} in the presence of Ca^{2+} during aggregation (first 40ns) are -1.29 and -0.87 $nm^2\ ns^{-1}$, respectively. The ratio of the above two rates is more than that of their unit numbers(4:3). Nonetheless, the length effect on the assembly dwindles in the presence of Na^+ since the decreasing rate also relies significantly on the way of accumulation. Interestingly, there is a drastic drop of surface area during 30 to 40 ns for PS_{n4} together with Ca^{2+}. From the configuration it is notable that the cluster contracts and changing its morphology.

Table 2. Average length, solvent accessible surface area (SASA), number of hydrogen bonds (HBs) between polysaccharide and water, number of intra-chain hydrogen bonds and number of inter-chain hydrogen bonds.

		PS_{n3} + Ca^{2+}	PS_{n3} + Na^+	PS_{n4} + Ca^{2+}	PS_{n4} + Na^+
Length (nm)		3.7	3.6	4.7	4.6
ΔSASA ($nm^2\ ns^{-1}$)		-0.87	-0.69	-1.29	-0.81
No. of HBs with solvent	Initial	717		934	
	Assembled	577	588	785	863
No. of intra-chain HBs	Initial	38.5		50	
	Assembled	26.3	32.4	18.3	35.8
No. of inter-chain HBs		20.6	26.4	43.7	38.6

The solvent accessible surface area (SASA) is defined as the surface formed by the spheres with each sphere centred on the corresponding atom with radius equal to $r_{vdw}+r_{sol}$, where r_{vdw} is the van der Waals radius of the atom and r_{sol} the radius of the solvent molecule. SASA is calculated with the GROMACS utility g_sas.[27] The hydrophobic area of a polymer is defined as the methyl groups in fucose. Data denoted as initial are averaged for the first 20-100 ps and those specified as assembled are sampled over the last 50 ns simulation. A hydrogen bond is formed when the donor-acceptor distance is within 3.25Å and the hydrogen-donor-acceptor angle is no more than 30°.

The assembling takes place either by forming hydrogen bonds or by tangling with van der Waals interactions between two chains or by coagulating through ionic bridges. The contraction of the hydrophobic domain results from the van der Waals attraction between the methyl groups in α-L-fucose. As shown in Fig 2, initially there are few other methyl groups surrounding the selected methyl group and the first distribution peak at 10Å originates from the neighboring units. As the polysaccharides assemble into the aggregate, a new distribution peak is found at 4Å. Although the polysaccharides possess a large proportion of

carbons, many of these hydrophobic constituents are buried by hydroxyl groups and not accessed by the solvent. Consequently, only one quarter of the SASA is hydrophobic, as seen in Table 2. The proportion of the hydrophobic domain in the contracted areas is consistent with that in the overall SASA and the percentage of hydrophobic domain in SASA is little changed after the assembly process, around 25%.

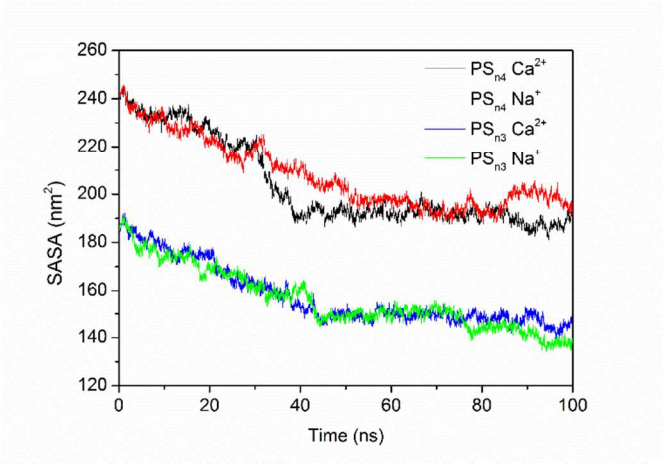

(a)

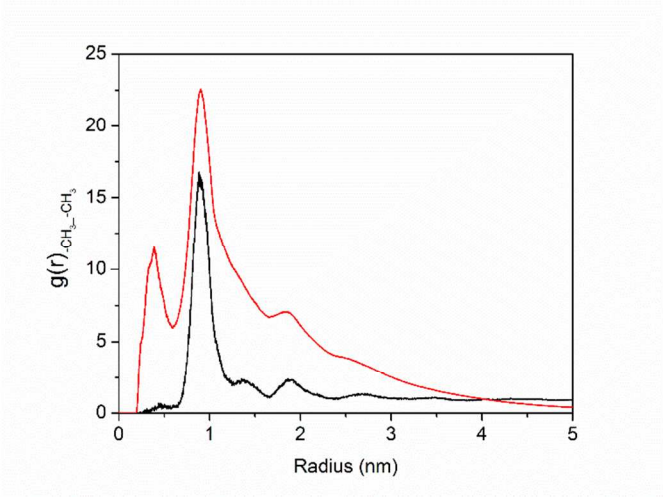

(b)

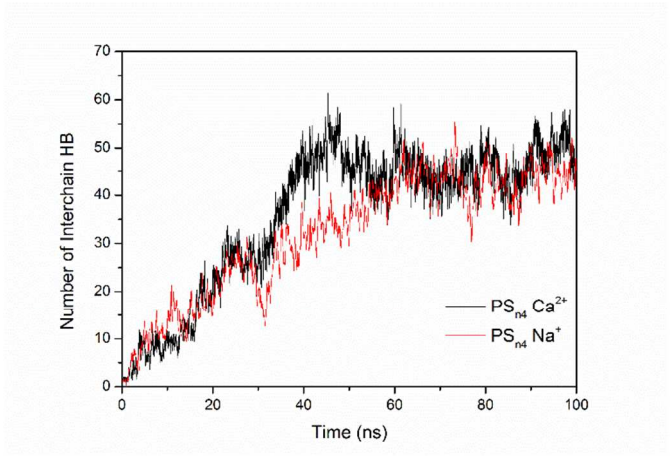

(c)

Figure 2. (a) Contraction of the SASA during aggregation. (b) Radial distribution function (RDF) of $-CH_3$ around other $-CH_3$. The black line and the red line depict the RDF before and after the assembly, respectively. (c) Inter-chain hydrogen-bond formation during aggregation.

The hydroxyl groups are mainly occupied by water or form intra-chain hydrogen bonds initially — 934 hydrogen bonds with water and 50 intra-chain hydrogen bonds are observed for the ten PS_{n4}. During self-assembly, an increasing interaction of polysaccharides with ions and a creation of inter-chain bonding are observed. We note that the creation of inter-chain hydrogen bonds follows exactly the opposite trend to the decrease of the SASA, as shown in Fig 2(c). For PS_{n4} in the presence of Ca^{2+}, the number of inter-chain hydrogen bonds is significantly enhanced during 30~40 ns, which is the time when the largest cluster of PS_{n4} contracts by shrinking its surface area. Moreover, since the hydrophilic domain dominates the polymer chain (75%), the inter-chain hydrogen bonds becomes more important than the tangling of the hydrophobic domain. In spite of the decreasing number of total hydrogen bonds, the number of hydrogen bonds for PS_{n4} with water decreases about 17%. Nevertheless, this value is smaller than the percentage of the contracted surface area in total SASA, 23%, implying that the aggregate becomes more adequately solvated.

3.2 Structure of aggregates

Albeit PS_{n4} possesses more inter-chain hydrogen bonds owing to more abundant hydroxyl groups, the aggregate of PS_{n4} is less compact in the absence of Ca^{2+}. From both the order parameter and the visual configuration, we can see clearly that the polysaccharides cannot align and that only a small part of the chains turns to bind one another during the assembly process (Fig S2 and S3 in Supplementary Information). Moreover, the aggregate has a gyration radius of 3.99 nm and is severely distorted with three components in the x, y, z direction being 5.87, 3.12, 1.71 nm. The less compact structure implicates that the long-chain polymers are more bent per se. The length of the polysaccharides is represented by the end-to-end distance. The average end-to-end distance for PS_{n4} is 4.70 nm in the presence of Ca^{2+}, while the corresponding value for PS_{n3} is 3.71 nm, as shown in Table 3. As shown in Fig 3(a), the end-to-end distance distribution of PS_{n4} extends from 2.8 to 5.4 nm, which is much wider than PS_{n3}. Moreover, the peak of PS_{n4} is observed to be diminished in the presence of Na^+, implying more flexibility. The more bent conformation is further verified

from the angle of the three consecutive oxygen atoms which act as the joints of the polymer. That the longer chain showing smaller angle suggests a higher probability for the chain to connect to itself, which may hinder the interaction with other polymer chains.

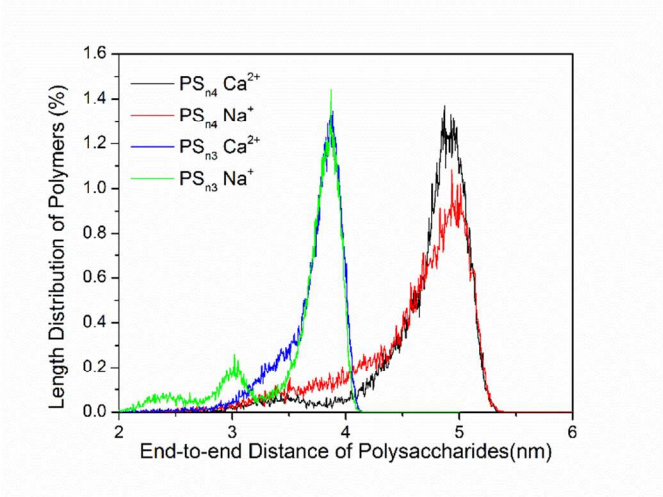

(a)

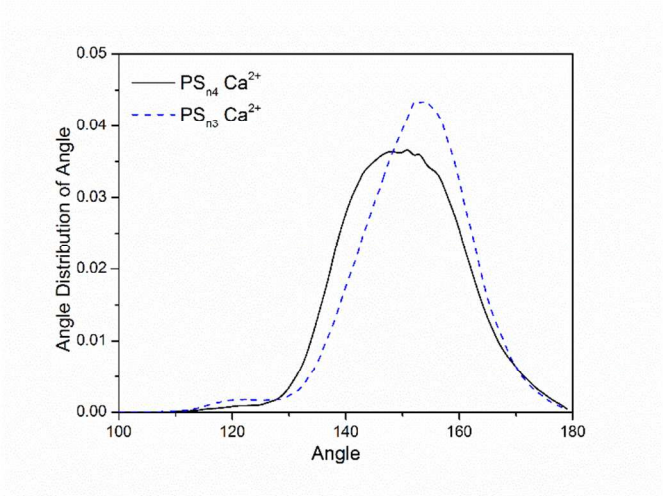

(b)

Figure 3. (a) End-to-end distance distribution of polysaccharides; (b) angle probability of two adjacent units. The angle is calculated as that of the three adjoining oxygen atoms acting as joints.

Table 3. Gyration radius, captured cations and surface tension of polysaccharide aggregates.

	PS_{n3} + Ca^{2+}	PS_{n3} + Na^{+}	PS_{n4} + Ca^{2+}	PS_{n4} + Na^{+}
Gyration radius (nm)	2.38	2.09	2.79	3.99
No. of captured cation	13	4	17	F5
γ(mJ m^{-2})	47.88±0.19	48.01±0.2	48.67±0.43	48.31±0.20
$\Delta\gamma$(mJ m^{-2})	0.45	0.26	1.24	0.48

Gyration radius is a parameter specifying the morphology of an aggregate. It is calculated as $r_{gyr} = \sqrt{\sum_i^N m_i r_i^2 / \sum_i^N m_i}$, where r denotes the distance of the i-th atom to the centre of mass of the N-atom system. Ions are regarded as captured by –COO$^-$ when ion-oxygen distance is smaller than 3.25Å. The surface tension of a planar interface is calculated through the diagonal components of the pressure tensor (P_{zz}, P_{xx}, P_{yy}): $\gamma_o = \frac{1}{2} L_Z \left[P_{zz} - \frac{1}{2}\left(P_{xx} + P_{yy}\right) \right]$.[28] The surface tension of pure water interface is estimated as 47.08 mJ m^{-2} while the increase of surface tension by adding $CaCl_2$ and NaCl is computed as 4.03 and 2.19 mJ m^{-2} L mol^{-1}, the latter of which accords with experiments.[29] $\Delta\gamma$ is calculated by excluding the influence from ions.

In the presence of Ca^{2+}, the cluster is less solvated with less hydrogen-bonded water around and the overall number of hydrogen bonds involving polysaccharides is smaller than that in the presence of Na^+. This is because Ca^{2+} interacts strongly with carboxyl groups. As shown in Fig4(a) and (b), it is apparent that both Ca^{2+} and Na^+ accumulate within the first coordinate shell of the -COO$^-$ residues, which is within 3 Å of the oxygen atom in the –COO$^-$ groups. The probability for –COO$^-$ to meet a Ca^{2+} ion is much higher with more Ca^{2+} distributing around the –COO$^-$ groups. Cations accumulate within the first hydration shell and interact directly with the negative charge. There are totally 17 Ca^{2+} but only 5 Na^+ around the assemblies of PS_{n4}.

Not only is the number of Ca^{2+} involved in the assemblies more dominant than that of Na^+, but they are also capable of attracting more than one negatively charged uronic acid. As seen from Fig4(c), Na^+ can hardly interact with more than one carboxyl group simultaneously, while the number of Ca^{2+} interacting with more than one carboxyl groups increases during aggregation. An increased length of polysaccharides enables more Ca^{2+} to act as ionic bridges. Moreover, the percentage of Ca^{2+} acting as ionic bridges increases from 36% for PS_{n3} to 42% for PS_{n4}, which further supports the significance of Ca^{2+} in long-chain assembling. It is also noteworthy that in the presence of Ca^{2+}, the number of the intra-chain hydrogen-bonds of the long-chain aggregate is distinctly diminished. This number is reduced to 18.3, compared with 35.8 in the absence of Ca^{2+}, as seen in Table 2. Moreover, the involvement of Ca^{2+} degrades the gyration radius of the long-chain aggregate to 2.79 nm, while the value is 3.99 nm in the presence of Na^+, as seen in Table 3. The assembly is thus more compact in the presence of Ca^{2+} and the influence of ionic bridges is more pronounced for PS_{n4}.

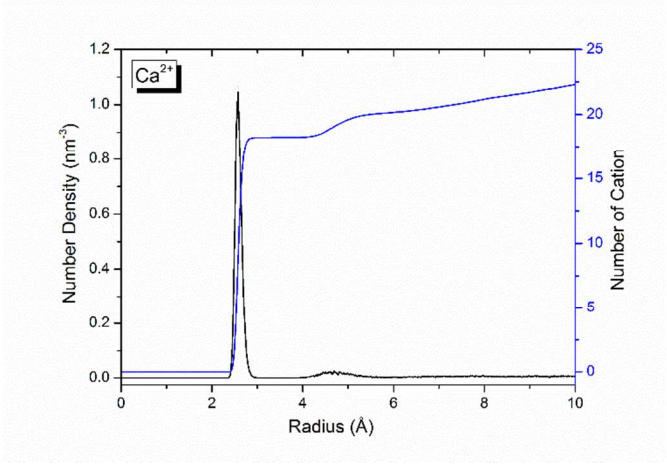

(a)

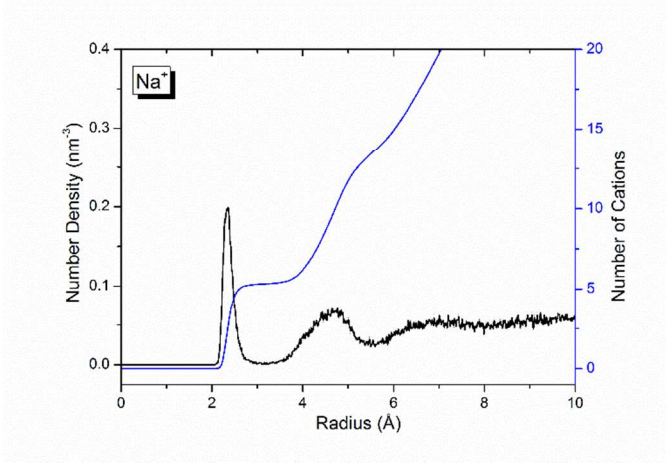

(b)

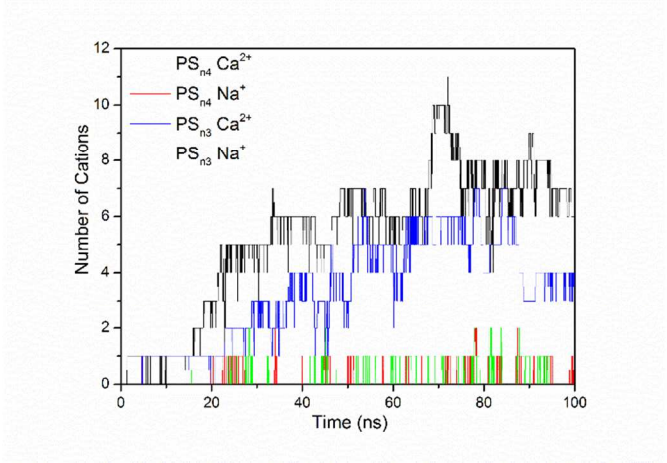

(c)

Figure 4. Number densities of (a) Ca^{2+} and (b) Na^{+} around the oxygen atoms of the $–COO^{-}$ residues in PS_{n4}. The density is averaged over the last 50 ns. (c) Number of cations that act as ionic bridges.

3.3 Interfacial properties

To shed light on the influence of the polysaccharides aggregates on the air/water interface, we calculated the surface tension for the corresponding planar surface, as shown in Table 3. Hereby we only compare the surface tension difference because the surface tension of pure water is calculated as 47.08 mJ m^{-2}, deviating from the experiments, 72.4 mJ m^{-2}.[30] All the systems with aggregates exhibit an increased surface tension. By eliminating the enhancement from the ions, the effects from assembly are shown as $\Delta\gamma$ in Table 2. The assembled structures affect the surface tension in different manners. In the presence of Ca^{2+}, the surface tension is enhanced by the aggregate more than that in presence of Na^{+}, especially for the studied four-unit chain polymer. The aggregate of PS_{n4} increases the surface tension by 1.24 mJ m^{-2} in the presence of Ca^{2+}, while this value is much smaller, 0.48 mJ m^{-2} in the absence of Ca^{2+}. The phenomenon accords with the gyration radius, as the aggregate of PS_{n4} is less compact in the absence of Ca^{2+}.

4. Conclusions

Recent unique results confirm for the first time that polymer gels in atmospheric aerosol particles and in cloud water originate from seawater[14b] and strongly suggest a link between cloud formation and polymer gels in the ocean surface microlayer (<1000 µm thick at the air-sea interface). However, the microscopic details of the polysaccharide assemble process into nanogels and the chemical properties involved remains largely unclear even after the application of most modern characterization techniques. This work tries to build an atomic insight into the self-assembly process of polysaccharides and to illustrate the influence of different cations and size of polymer chains. It is shown that the polymers assemble quickly with two distinct ways to grow; by forming small clusters and aggregating into one or by absorbing the dissolved polymers one by the other. The latter process requires less time to assemble. The elongated length of a polymer chain accelerates the assembly process and the contraction of the solvent accessible surface area. Hydrophilic areas contract more distinctly though the proportions of the hydrophobic and hydrophilic areas remain basically the same after assembling. The inter-chain hydrogen bonds are significant for the assembly process and are the main driving force to induce the solvent accessible surface area contraction. The longer polymer studied is observed to be more bent and less compact with a much bigger gyration radius. The involvement of Ca^{2+} is found to promote the order of assembly of four-unit polysaccharides with less intra-chain hydrogen bonds and a reduced gyration radius. Moreover, the percentage of Ca^{2+} behaving as ionic bridges is promoted in the longer chains compared with the short chains. We thus find that the importance of Ca^{2+} is strengthened for the long-chain assembly and in forming ionic bridges. Since the aggregates are rendered as more compact structures in the presence of Ca^{2+}, the surface tension is quite significantly enhanced. The formation of such branched, fractal-like assemblies is favored in the surface microlayer, and such microgels can be injected into the atmosphere from the uppermost sea surface and subsequently be activated into fog- and cloud water where they could undergo both phase volume transition by changes in pH and fragmentation into nanogels by UV-light.[14b] During evaporation events, where nano-granules appear, this study implies that a faster way of aggregating is by adding saccharide units one after another, forming more stable and compact structures, which is in line with experimental

observations.[16] An enhancement of the surface tension as a result of Ca^{2+} ions further favors a branched, fractal structure. We believe that these results add to the understanding of the assembly of polysaccharides into marine gels and hope this understanding will keep up interest in the complex but fascinating interactions between marine microbiology and research on atmospheric aerosols, clouds and climate.

Acknowledgements

The authors thank the Swedish Infrastructure Committee (SNIC) for providing computational resources for the project "Multi-physics Modeling of Molecular Materials", SNIC2013-26-31. L.S. thanks the China Scholarship Council for financial support.

Notes and references

[a] Department of Theoretical Chemistry and Biology, School of Biotechnology, Royal Institute of Technology, S-10691 Stockholm, Sweden

[b] Department of Meteorology, Stockholm University, S-10691Stockholm, Sweden.

Electronic Supplementary Information (ESI) available: Supplementary potential energies among polymers and ions, order parameters and visual configurations of ionic bridge and hydrogen bonds inside the assembly are listed in Supplementary Information. This material is available free of charge via the Internet at http://pubs.acs.org.

1 G. L. Stephens, *J. Climate.*, 2005, **18**, 37.
2. H. Köhler, *T. Faraday Soc.*, 1936, **32**, 1152-1161.
3. a)R. Sorjamaa, B. Svenningsson, T. Raatikainen, S. Henning, M. Bilde and A. Laaksonen, *Atmos Chem Phys*, 2004, **4**, 2107-2117; b)P. Chakraborty and M. R. Zachariah, *J. Phys. Chem. A*, 2008, **112**, 966-972.
4. a)E. K. Bigg, *J. Appl. Meteorol.*, 1980, **19**, 521-533; b)C. Leck, M. Norman, E. K. Bigg and R. Hillamo, *J. Geophys. Res-Atmos.*, 2002, **107**.
5. a)M. V. Orellana, E. J. Lessard, E. Dycus, W. C. Chin, M. S. Foy and P. Verdugo, *Mar. Chem.*, 2003, **83**, 89-99; b)R. Benner, J. D. Pakulski, M. Mccarthy, J. I. Hedges and P. G. Hatcher, *Science*, 1992, **255**, 1561-1564; c)D. A. Hansell, C. A. Carlson, D. J. Repeta and R. Schlitzer, *Oceanography*, 2009, **22**, 202-211.
6. G. G. Leppard, M. M. West, D. T. Flannigan, J. Carson and J. N. A. Lott, *Can. J. Fish. Aquat. Sci.*, 1997, **54**, 2334-2349.
7. P. H. Santschi, E. Balnois, K. J. Wilkinson, J. W. Zhang, J. Buffle and L. D. Guo, *Limnol. Oceanogr.*, 1998, **43**, 896-908.
8. a)M. V. Orellana, T. W. Petersen, A. H. Diercks, S. Donohoe, P. Verdugo and G. van den Engh, *Mar. Chem.*, 2007, **105**, 229-239; b)W. C. Chin, M. V. Orellana and P. Verdugo, *Nature*, 1998, **391**, 568-572.
9. P. Verdugo, *Annu. Rev. Mar. Sci.*, 2012, **4**, 375-400.
10. a)D. C. Blanchard, *Prog. Oceanogr.*, 1963, **1**, 73-202; b)D. C. Blanchard and A. H. Woodcock, *Tellus*, 1957, **9**, 145-158; c)E. K. Bigg and C. Leck, *J. Geophys. Res-Atmos.*, 2008, **113**.
11. a)E. K. Bigg and C. Leck, *J. Geophys. Res-Atmos.*, 2001, **106**, 32101-32109; b)C. Leck and E. K. Bigg, *Geophys. Res. Lett.*, 2005, **32**.
12. E. K. Bigg, C. Leck and L. Tranvik, *Mar. Chem.*, 2004, **91**, 131-141.
13. E. K. Bigg, *Environ. Chem.*, 2007, **4**, 155-161.
14. a)C. Leck and E. K. Bigg, *Environ. Chem.*, 2007, **4**, 400-403; b)M. V. Orellana, P. A. Matrai, C. Leck, C. D. Rauschenberg, A. M. Lee and E. Coz, *P. Natl. Acad. Sci. USA*, 2011, **108**, 13612-13617; c)C. Leck, Q. Gao, F. M. Rad and U. Nilsson, *Atmos. Chem. Phys.*, 2013, **13**, 12573-12588.
15. a)C. Leck and E. K. Bigg, *Geophys. Res. Lett.*, 1999, **26**, 3577-3580; b)C. Leck and E. K. Bigg, *Aerosol Sci. Tech.*, 2010, **44**, 570-577; c)M. Karl, C. Leck, A. Gross and L. Pirjola, *Tellus B*, 2012, **64**.
16. M. Karl, C. Leck, E. Coz and J. Heintzenberg, *Geophys. Res. Lett.*, 2013, **40**, 3738-3743.
17. X. Li, C. Leck, L. Sun, T. Hede, Y. Q. Tu and H. Agren, *J. Phys. Chem. Lett.*, 2013, **4**, 2637-2642.
18. a)O. Smidsrod, *Faraday Discuss.*, 1975, **57**, 263-+; b)J. A. Hornemann, A. A. Lysova, S. L. Codd, J. D. Seymour, S. C. Busse, P. S. Stewart and J. R. Brown, *Biomacromolecules*, 2008, **9**, 2322-2328.
19. B. Hess, C. Kutzner, D. van der Spoel and E. Lindahl, *J. Chem. Theory Comput.*, 2008, **4**, 435-447.
20. M. I. Bilan, E. V. Vinogradova, A. S. Shashkov and A. I. Usov, *Phycologia*, 2005, **44**, 9-9.
21. P. Verdugo, A. L. Alldredge, F. Azam, D. L. Kirchman, U. Passow and P. H. Santschi, *Mar. Chem.*, 2004, **92**, 67-85.
22. S. F. Edwards, *J. Polym. Sci. Pol. Sym.*, 1985, R9-R12.
23. a)B. L. Foley, M. B. Tessier and R. J. Woods, *WIREs Comput. Mol. Sci.*, 2012, **2**, 652-697; b)K. N. Kirschner, A. B. Yongye, S. M. Tschampel, J. Gonzalez-Outeirino, C. R. Daniels, B. L. Foley and R. J. Woods, *J. Comput. Chem.*, 2008, **29**, 622-655; c)W. D. Cornell, P. Cieplak, C. I. Bayly, I. R. Gould, K. M. Merz, D. M. Ferguson, D. C. Spellmeyer, T. Fox, J. W. Caldwell and P. A. Kollman, *J. Am. Chem. Soc.*, 1996, **118**, 2309-2309; d)W. L. Jorgensen, J. Chandrasekhar, J. D. Madura, R. W. Impey and M. L. Klein, *J. Chem. Phys.*, 1983, **79**, 926-935.
24. a)G. Bussi, D. Donadio and M. Parrinello, *J. Chem. Phys.*, 2007, **126**; b)H. J. C. Berendsen, J. P. M. Postma, W. F. Vangunsteren, A. Dinola and J. R. Haak, *J. Chem. Phys.*, 1984, **81**, 3684-3690.
25. a)B. Hess, H. Bekker, H. J. C. Berendsen and J. G. E. M. Fraaije, *J. Comput. Chem.*, 1997, **18**, 1463-1472; b)B. Hess, *J. Chem. Theory. Comput.*, 2008, **4**, 116-122.
26. a)T. Darden, D. York and L. Pedersen, *J. Chem. Phys.*, 1993, **98**, 10089-10092; b)U. Essmann, L. Perera, M. L. Berkowitz, T. Darden, H. Lee and L. G. Pedersen, *J. Chem. Phys.*, 1995, **103**, 8577-8593.
27. F. Eisenhaber, P. Lijnzaad, P. Argos, C. Sander and M. Scharf, *J. Comput. Chem*, 1995, **16**, 273-284.
28. J. Alejandre, D. J. Tildesley and G. A. Chapela, *J. Chem. Phys.*, 1995, **102**, 4574-4583.
29. M. J. Hey, D. W. Shield, J. M. Speight and M. C. Will, *J. Chem. Soc. Farad. T 1*, 1981, **77**, 123-128.
30. D. R. Lide and H. P. R. Frederikse, *CRC Handbook of Chemistry and Physics*, 79 edn., CRC Press, Baco Raton, 1998.